

**Static magnetic order with strong quantum fluctuations in spin-1/2 honeycomb
magnet $\text{Na}_2\text{Co}_2\text{TeO}_6$**

Gaotong Lin^{1#}, Jinlong Jiao^{1#}, Xiyang Li^{2#}, Mingfang Shu¹, Oksana Zaharko³, Toni Shiroka^{4,5}, Tao Hong⁶, Alexander I. Kolesnikov⁶, Guochu Deng⁷, Sarah Dunsiger^{8,9}, Haidong Zhou¹⁰, Tian Shang^{11*}, and Jie Ma^{1*}

¹*Key Laboratory of Artificial Structures and Quantum Control, Shenyang National Laboratory for Materials Science, School of Physics and Astronomy, Shanghai Jiao Tong University, Shanghai 200240, China*

²*Quantum Matter Institute, University of British Columbia, Vancouver, British Columbia V6T 1Z4, Canada*

³*Laboratory for Neutron Scattering and Imaging, Paul Scherrer Institut, Villigen, Switzerland*

⁴*Laboratory for Muon-Spin Spectroscopy, Paul Scherrer Institut, Villigen PSI, Switzerland*

⁵*Laboratorium für Festkörperphysik, ETH Zürich, CH-8093 Zürich, Switzerland*

⁶*Neutron Scattering Division, Oak Ridge National Laboratory, Oak Ridge, TN 37831, USA*

⁷*Australian Centre for Neutron Scattering, Australian Nuclear Science and Technology Organization, New Illawarra Road, Lucas Heights, NSW 2234, Australia*

⁸*Department of Physics, Simon Fraser University, Burnaby, BC, V5A 1S6, Canada*

⁹*Centre for Molecular and Materials Science, TRIUMF, Vancouver, BC, V6T 2A3, Canada*

¹⁰*Department of Physics and Astronomy, University of Tennessee, Knoxville, Tennessee 37996, USA*

¹¹*Key Laboratory of Polar Materials and Devices (MOE), School of Physics and Electronic Science, East China Normal University, Shanghai 200241, China*

These authors contributed equally to this work.

*Corresponding author: tshang@phy.ecnu.edu.cn
jma3@sjtu.edu.cn

Abstract

Kitaev interaction, an interplay from frustrated bond anisotropy, can lead to strong quantum fluctuations and thus quantum spin liquid state in an ideal Kitaev model. However, the presence of the non-Kitaev interactions usually promotes the ground state to a zigzag antiferromagnetic order in *d*-orbital transition metal Kitaev candidates. Combining with the neutron scattering and the muon-spin rotation and relaxation techniques, we provided further insights into nature of the exotic properties of $\text{Na}_2\text{Co}_2\text{TeO}_6$, and found that the zero-field muon-spin relaxation rate becomes approximately constant with a value close to $0.45 \mu\text{s}^{-1}$ at temperatures below T_N . Such a temperature-independent muon-spin relaxation rate is most likely attributed to the presence of strong quantum fluctuations as well as the frustrated Kitaev interaction. As the magnetic field is increased, a spin-wave-excitation gap at K-point becomes much broader. Therefore, the quantum fluctuations are quite robust and even can be enhanced by applying magnetic field, which would help us further understand the possible quantum-spin-liquid state in a Kitaev candidate.

The Kitaev model was introduced in a spin-1/2 two-dimensional (2D) honeycomb lattice as an exactly solvable 2D spin model that achieves a quantum-spin-liquid (QSL) ground state [1], and has attracted tremendous attention. Both theoretical and experimental practices have been attempted to search for a QSL candidate with dominant bond-dependent anisotropic-exchange interactions, named, Kitaev interaction K term [2-18]. Up to date, the Kitaev model is successfully realized in the $3d/4d/5d$ transition metal families of materials [8-13,18-21], however, owing to the existence of non-Kitaev interactions [6,7,13,15], e.g., the Heisenberg exchanges, the off-diagonal symmetric interactions Γ and Γ' terms, most of these materials exhibit a zigzag antiferromagnetic (AFM) order at low temperatures in the absence of magnetic field.

Compared to the earlier recognized $4d/5d$ Ru/Ir systems with strong spin-orbit coupling (SOC) [15-17], the $3d$ Co-based Kitaev QSL candidates are still highly controversial that continues today [12,13,19,22-28]. In $3d$ -based candidates of the Kitaev model, $\text{Na}_2\text{Co}_2\text{TeO}_6$ (NCTO) has been realized as one of the most prominent examples to study Kitaev physics [12,13,15,19,28-35]. Although the evidence of field-induced QSL has been obtained [13,19,36,37], the magnetic structure of the ground state still remains an urgent problem to be solved [13,19,26,27,31,33,38], which will be helpful to further understand the competitors of K , such as various Heisenberg interactions like the nearest-neighbor (NN) Heisenberg coupling J_1 and the third NN Heisenberg coupling J_3 .

Recently, researchers start to make different analysis on the magnetic structure of NCTO through various experimental methods, such as single-crystal or powder neutron diffractions, nuclear magnetic resonance, and electrical polarization measurements [26,27,29-31,39,40], while an uncontroversial result is still not obtained. i) The powder neutron diffraction experiments suggest a zigzag AFM order lying in the ab plane [see Figure 1(a)], accompanied by a Néel-type canting along the c axis at $T_N \sim 26$ K [39,40], however, a novel triple- q order (or multi- k structure) at 0 T was suggested by the single-crystal neutron diffraction [12,27,28,31]. ii) Although the field-dependence of the

characteristic magnetic reflections (0.5, 0, 1) and (0, 0.5, 1) demonstrated the magnetic multi-domain effect of the zigzag AFM [27], the temperature dependence of the magnetic reflection (0.5, 0, 0) is not sufficient to exclude the triple- q order [12,27,31]. iii) The spin-dynamics were analyzed by a generalized Heisenberg–Kitaev (HK) model with five symmetry-allowed terms: K term, Γ and Γ' terms, J_1 , and J_3 [13,33–35,41], and two different exchange frustrations, namely J_1 - J_3 -type and Kitaev-type frustrations, made the determination of the ground state rather difficult. To distinguish those two magnetic structures, multi-domain or multi- k structure, it is better to measure the field- and temperature-dependent magnetic reflections and the related dynamics at the series of the M-points in the ab -plane, such as M (0.5, 0, L), M_1 (-0.5, 0.5, L), and M_2 (0, 0.5, L) where L is an arbitrary integer along the c -axis, shown in the Figure 1(b).

In this letter, we studied the nature of the zigzag AFM order in NCTO single crystal via the neutron scattering and the muon-spin rotation and relaxation (μ SR) techniques. The differences from the temperature and magnetic field dependence of the characteristic magnetic reflections M (0.5, 0, 1) and M_1 (-0.5, 0.5, 1) indicate that the magnetic ground state presents a multi-domain structure, rather than a multi- k structure. Below T_N , the modulation of magnetic domains induces the other two transitions at T_F and T^* , which are also reflected by the temperature dependence of weak transverse-field (wTF) μ SR asymmetry and zero-field (ZF) muon-spin relaxation rate. Furthermore, the estimated static magnetic volume fraction ($\sim 90\%$) confirms the high quality of NCTO single crystals. The temperature-dependent muon-spin relaxation rate in the AFM state implies the presence of strong quantum spin fluctuations.

The measurements were performed on high-quality single crystals grown by a flux method described in Ref. [19]. A piece of NCTO single crystal ($\sim 10\text{mg}$), inset of Fig. S1(a), was used for the neutron diffraction experiment with the Thermal Single Crystal Diffractometer ZEBRA at the Swiss Neutron Spallation Source SINQ, Paul Scherrer Institut (PSI), Switzerland. For the measurements on ZEBRA, a neutron wavelength of 1.383 Å was used for all measurements, provided by the Ge monochromator. In-field data were collected within a lifting arm normal-beam geometry where the crystal was

inserted in a vertical 10 T magnet, Fig. S1 [42]. The magnetic states were investigated under a principal field configuration $B \parallel [-1 \ 1 \ 0]$ (equivalent to \mathbf{a}^* -axis). Spin-wave-excitation spectra were measured using the SEQUOIA time-of-flight spectrometer at the Spallation Neutron Source, Oak Ridge National Laboratory, USA [43,44]. The constant-Q scans of the K-point $(1/3, 1/3, 0)$ at 1.5 K with applied field B up to 4 T and $B \parallel [-1,1,0]$ direction were measured on the Cold Triple Axis Spectrometer SIKA at the ANSTO, Australia [45]. About 0.559 g samples for SEQUOIA and 0.6 g samples for SIKA were glued on the aluminum sheets, and co-aligned in the (HHL) scattering plane with $\mathbf{B} \parallel [-1,1,0]$ direction by a backscattering Laue x-ray diffractometer [42]. The zero-field (ZF), longitudinal-field (LF), and wTF- μ SR experiments were performed on the M20D surface muon beam line at TRIUMF in Vancouver, Canada using the LAMPF spectrometer [42]. In addition, the wTF- μ SR experiments were also carried out at the general-purpose surface-muon (GPS) instrument at the π M3 beam line of the Swiss muon source (S μ S) at PSI in Villigen, Switzerland [42]. All these μ SR spectra were analyzed by means of the musrfit software package [46].

To determine whether the magnetic ground state of NCTO is a multi-domain structure or a multi- k structure, both the temperature- and magnetic-field dependence of the magnetic reflections M $(0.5, 0, 1)$ and M_1 $(-0.5, 0.5, 1)$ were measured for the k vectors of $(0.5, 0, 0)$ and $(-0.5, 0.5, 0)$, respectively [see Figure 1(c) and (d)]. The differences of unnormalized intensity magnitudes at the M and M_1 points may be due to the non-spherical sample morphology (see the measured sample in Fig. S1 [42]). In addition, tiny differences were observed from the temperature dependence of intensity $I(T)$ curves at M and M_1 points. The $I(T)$ curve at the M -point can be well fitted by a power-law function: $I(T) = I_0 \cdot [1 - (T/T_N)]^{2\beta}$ [47], which confirmed the magnetic phase transition temperature $T_N \approx 26$ K and the critical exponent of the order parameter $\beta \approx 0.22$. With the same values of T_N and β , the $I(T)$ curve at the M_1 -point can be also fitted by a power-law function, apart from a small bump near $T_F \approx 15$ K. Such consistency of the power-law function suggests that the anomaly at T_F may not be related to the magnetic phase transition. Indeed, the temperature dependence of the spin-wave-

excitation gap decreases with increasing temperature and vanishes exactly near T_F [31]. The appearance of the spin-wave-excitation gap can be attributed to the magnetic anisotropic-exchange interactions K and Γ terms originated from the SOC in NCTO [13], which may induce the non-equivalent magnetic domains with the different k vectors at the M and M_1 points. Hence, the subtle differences between these two magnetic reflections indicate that the magnetic ground state is a multi-domain structure, that is, the domains corresponding to the k vectors $(0.5, 0, 0)$ and $(-0.5, 0.5, 0)$ are not equally populated. Meanwhile, the yielded $\beta \approx 0.22$ falls between the ideal 2D Ising ($\beta = 0.125$) and 3D Ising ($\beta = 0.326$) system [48], which is consistent with the previous reports of the quasi-2D magnetic correlation [13,19,31].

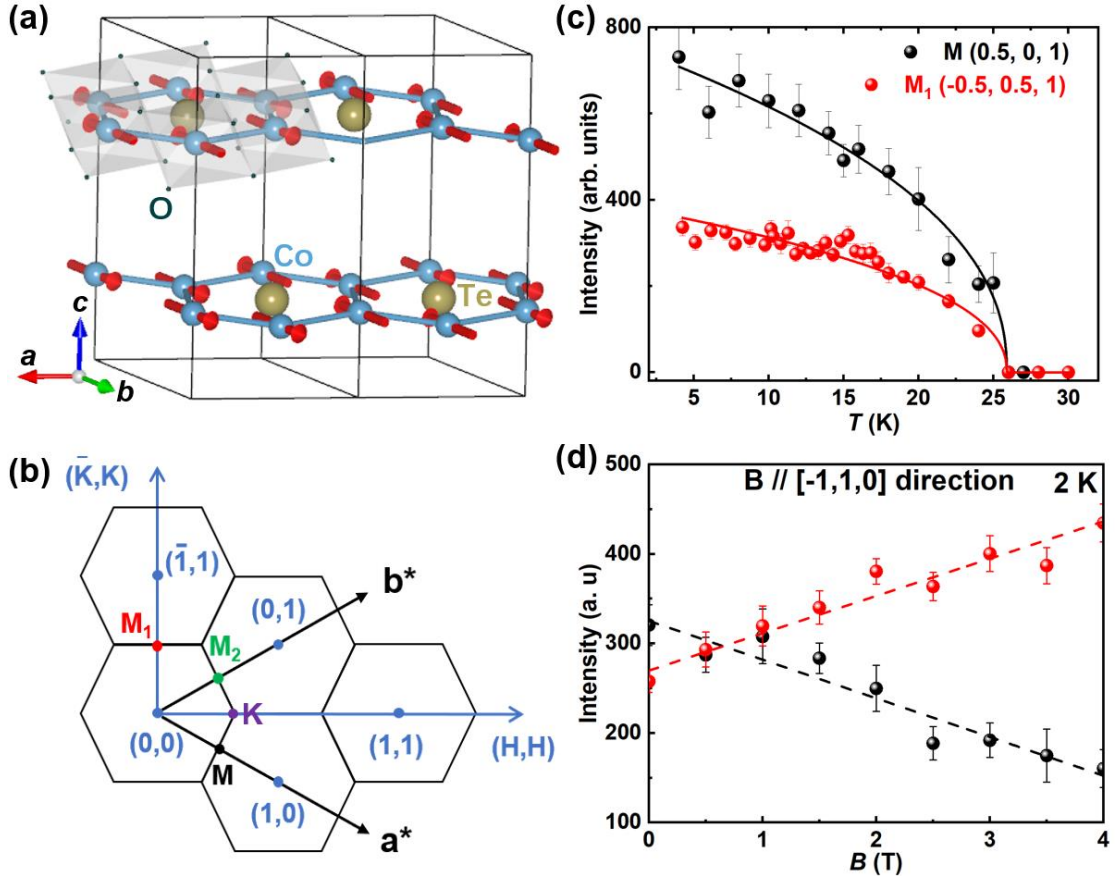


Figure 1. The honeycomb magnetic structure and single-crystal neutron diffraction results for NCTO. (a) Magnetic structure of NCTO, the domain characterized by the propagation vector of $(0.5, 0, 0)$ is presented. (b) Schematics of the Brillouin zones with the high symmetry points M , M_1 , M_2 , and K denoted by black, red, green, and purple dots, respectively, in the ab plane. The high symmetry points are equivalent at the integers of L along the c -axis and L is not shown in the figure. The magnetic field is applied along $[-1, 1, 0]$ direction (equivalent to the a^* -axis). (c), (d) The temperature dependence at 0

T and magnetic field dependence at 2 K of the intensities of two magnetic reflections at M (0.5, 0, 1) and M_1 (-0.5, 0.5, 1), where the solid curves in (c) are power-law fits to the data (described in the text) while the dash lines in (d) are just guide lines. (c) and (d) were both measured on the Thermal Single Crystal Diffractometer ZEBRA at the PSI, Switzerland.

As shown in Figure 1(d), the multi-domain structure is further supported by the magnetic-field dependence of intensity $I(B)$ curves at the magnetic reflections M and M_1 with the $\mathbf{B} \parallel [-1, 1, 0]$ -direction (equivalent to \mathbf{a}^* -axis) and $T = 2$ K. These two reflections exhibit completely different field-dependent behaviors. When increasing the magnetic field, the intensity of the M-point gradually decreases while that of the M_1 -point increases, indicating that the macroscopic symmetry is broken in the presence of magnetic field and the magnetic domains along the field direction gradually grow while domains in other directions are suppressed [49]. This evidence decisively discriminates multi-domain and multi- k structures. With the application of an external constraint (magnetic field or uni-axial stress), each arm of k vector exhibits distinct behavior under multi-domain conception, while they respond equally with multi- k scheme [50-53]. It is worth mentioning that the zigzag AFM ground state of NCTO exhibits a 2-fold symmetric angular dependence in the magnetic torque experiment under the low fields [19], which corresponds to the different $I(B)$ features at the magnetic reflections M and M_1 points.

Another feature of the quantum fluctuations usually could be demonstrated by the broadening of the spin-wave-excitation spectra in some strong quantum magnets [54-56]. In order to search for the quantum fluctuations under magnetic fields, we perform the single-crystal INS measurements by applying various magnetic fields up to 4 T along [-1,1,0] direction. As shown in Figure 2(a) and (b), one can see the obvious spin-wave band at 0 T and 4 T along the high symmetry momentum directions Γ -K-M path marked with the white arrows in the inset of Figure 2. At zero field, a gapped magnon band at the M-point reaches the minimum energy value of the band and has the largest intensity as expected, supporting the zigzag AFM order driven primarily by non-Kitaev interactions [12,19]. Compared to the lowest-energy spin-wave-excitation spectra at 0 T, the spin-wave band at 4 T, Figure 2(b), shows similar features but is accompanied by

a significant broadening. Note that we do not observe the phenomenon that the spin wave is split into multiple branches under the magnetic field. Hence, such broadening should be from the field-induced quantum fluctuations. At the same time, the field-induced quantum fluctuations are also confirmed by the constant-Q scans at the K-point, Figure 2(c), which presents a large excitation gap centered near 3 meV at 0 T [12,19]. With the increasing field up to 4 T, the zigzag AFM order is still stable, as indicated by the $I(B)$ curves of Figure 1(d), the shapes of the peaks in Figure 2(c) are gradually broadening. The field dependence of the full width at half maxima (FWHM) is plotted in the inset of Figure 2(c). These results indicate that the quantum fluctuations can be enhanced by the applied magnetic field in NCTO, which perfectly mirrors the field-induced magnetically disordered state with strong quantum fluctuations between about 7.5 T and 10 T with $\mathbf{B} \parallel \mathbf{a}^*$ -axis [13,19,37].

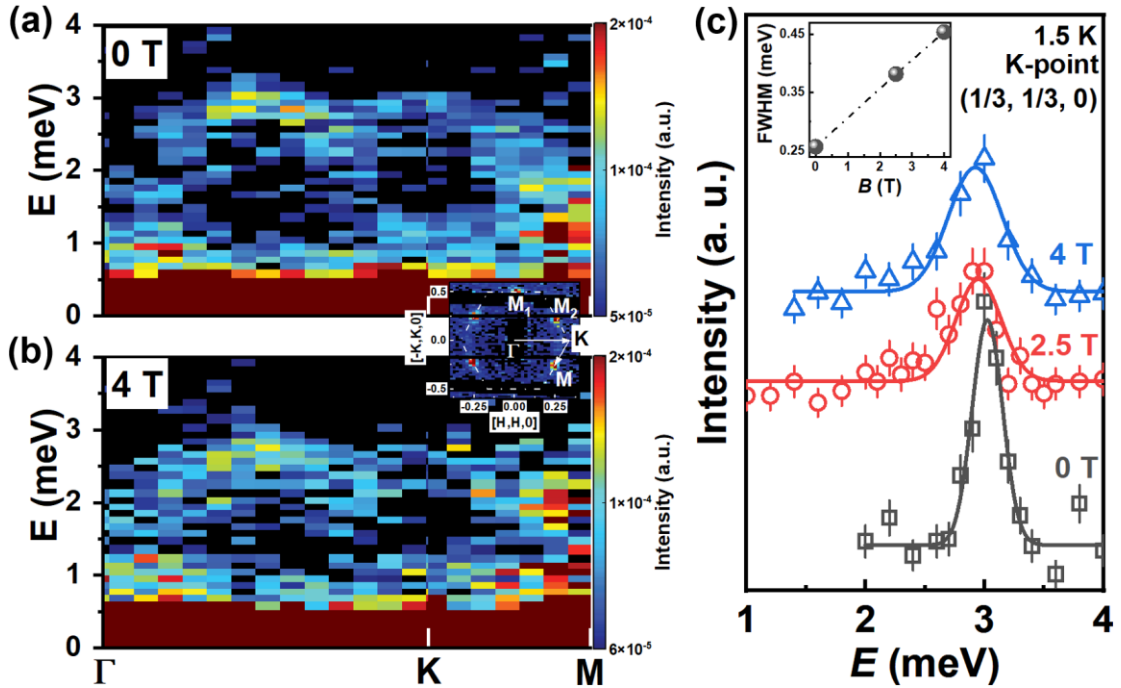


Figure 2. Single-crystal inelastic neutron scattering results for NCTO. (a) and (b) Lowest-energy spin-wave-excitation spectra at 2 K for 0 T and 4 T, respectively, along high symmetry momentum directions Γ -K-M path marked with the white arrows in the inset and using fixed incident energy $E_i = 18$ meV with $\mathbf{B} \parallel [-1,1,0]$ direction. The color bar indicates scattering intensity with arbitrary unit in linear scale. The inset shows that the elastic neutron scattering results integrated over $L = [-2.5, 2.5]$ and $E = 0 = \pm 0.075$ meV at 0 T using fixed incident energy $E_i = 60$ meV. The white dashed lines represent the Brillouin zone boundaries. The high symmetry points Γ , K, M, M_1 and M_2 are marked in the inset. (c) The constant-Q scans of the K-point $(1/3, 1/3, 0)$ at 1.5 K with applied field B up to 4 T and $\mathbf{B} \parallel [-1,1,0]$

direction. The solid lines are obtained by the Gaussian function fit. The inset shows the field dependence of the full width at half maxima (FWHM) from the fitted results. (a), (b), and inset were collected using the SEQUOIA chopper spectrometer while (c) was measured on SIKA spectrometer.

As an extremely sensitive probe for investigating complex quantum magnetism, μ SR could measure magnetic ordering at a microscopic level. The combination of the neutron scattering and μ SR techniques will help us to further verify the multi-domain structure and the quantum fluctuations in NCTO single crystal.

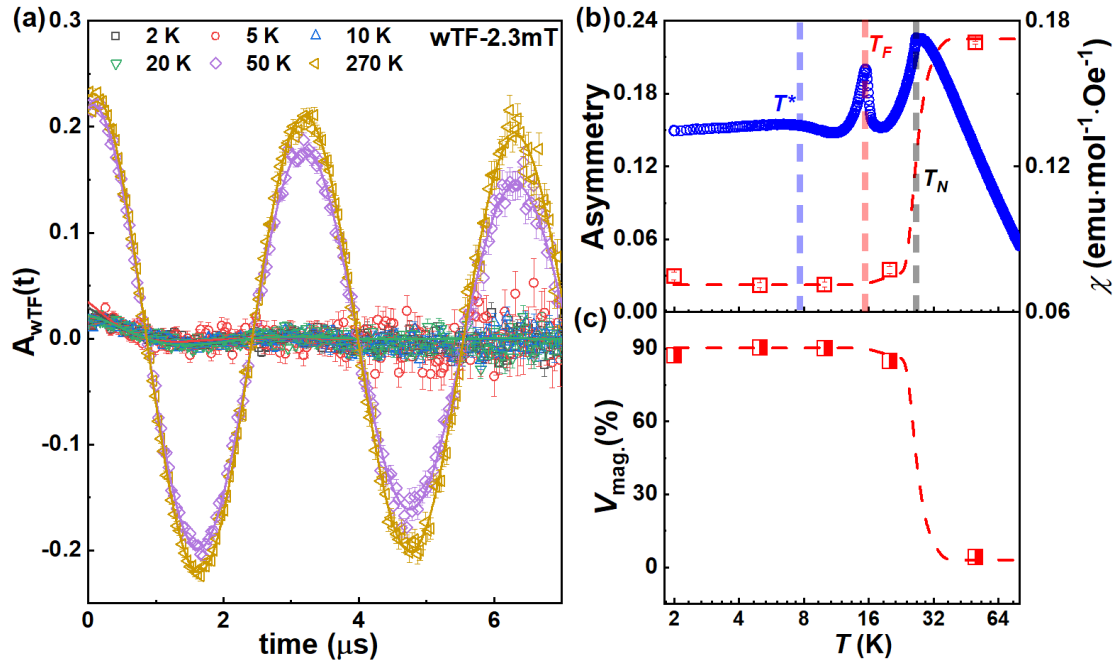


Figure 3. The study of magnetic phase transition and volume fraction measured by the wTF- μ SR spectra in NCTO. (a) Time-domain wTF- μ SR spectra were collected at different temperatures with a weak transverse field of 2.3 mT, which was acquired at M20D spectrometer. The solid lines are the fitted results by the Eq. (1); In order to clearly observe the oscillation characteristics of (a) below T_N , the time-domain wTF- μ SR spectra are also plotted in Fig. S7 [42]. (b) Temperature-dependent A_{NM} asymmetry (left axis and red symbols) was obtained from the fit of wTF- μ SR spectra. For comparison, we present the zero-field cooling (ZFC) magnetic susceptibility $\chi(T)$ curve at $B = 0.01$ T (right axis and blue symbols) with $\mathbf{B} \parallel \mathbf{a}^*$ -axis; The magnetic susceptibility data were taken from Ref. [19]. (c) The estimated magnetic volume fraction versus temperature. The red dash lines of (c) and (d) are the guidelines.

A quantitative analysis from wTF- μ SR spectra allows extracting the temperature evolution of the magnetic volume fraction and determining the magnetic transition temperatures. The external field of $B = 2.3$ mT was applied perpendicular to the initial muon-spin direction, which leads to a precession of the muon-spin with a frequency of

$\gamma_\mu B$ ($\gamma_\mu = 2\pi \times 135.5$ MHz/T is the muon's gyromagnetic ratio), as shown in Figure 3(a). It is noted that 2.3 mT field is much smaller than the internal fields induced by a long-range magnetic order in NCTO single crystal (see Fig. 4 below). Therefore, such a muon-spin precession reflects only the non-magnetic part of the sample, and the sample with a long-range magnetic order leads to a very fast muon-spin depolarization in the first tenths of μ s. As a consequence, the wTF- μ SR spectra can be described using the below function, without considering the very fast relaxation:

$$A_{wTF}(t) = A_{NM} \cos(\gamma_\mu B_{\text{int}} \cdot t + \varphi) e^{-\lambda t}, \quad (1)$$

where A_{NM} is the initial muon-spin asymmetry for muons implanted in the nonmagnetic (NM) or paramagnetic (PM) fraction of NCTO single crystals; B_{int} is the local field sensed by muons (here almost identical to the applied magnetic field); φ is the initial phase and λ is the muon-spin relaxation rate.

Figure 3(b) presents the temperature dependence of the asymmetry for the wTF- μ SR spectra. Below T_N , a static spin component leads to a fast reduction of asymmetry. Hence, A_{NM} starts to decrease quickly near the onset of an AFM order, which is consistent with the magnetic susceptibility data. Another broad weak peak from the wTF-5mT data, Fig. S3 [42], was also observed at a temperature close to T_F . Although NCTO undergoes three successive AFM transitions (indicated by dash lines in Figure 3(b)), the $A_{NM}(T)$ curve does not capture the possible phase transition at T^* [13]. This reflects that the internal field or magnetic structure is not significantly modified around T^* . When a perfect magnetically ordered ground state occurs at zero kelvin, the magnetic volume fraction V_{mag} will be close to 100% [57,58]. The temperature dependence of the magnetic volume fraction can be estimated from $V_{\text{mag}}(T) = 1 - A_{NM}(T)/A_{NM}(T > T_N)$, Figure 3(c). The estimated static magnetic volume fraction is up to 90% and the spin-glass behaviors revealed by the ac susceptibility measurements are absent in our NCTO crystals [26]. These results indicate that NCTO can be considered as fully magnetically ordered below T_N , indicative a high sample quality.

If the electronic magnetic moments fluctuate very fast (typically above 10^{12} Hz in the PM state), the muon-spin polarization would not be influenced. When the system

starts to enter the magnetically ordered state, the fluctuations of electronic magnetic moments are much smaller than the 10^{12} Hz, which will present a fast depolarization and superimposed oscillations reflecting the coherent precession of the muon polarization and the appearance of static magnetic moments. Figure 4(a) and (b) show plots of the ZF- μ SR time spectra for both $S_\mu \parallel \mathbf{a}$ -axis and $S_\mu \parallel \mathbf{c}$ -axis. Such fast depolarization and superimposed oscillations within 50 ns originated from the AFM order (also see the Fig. S4 [42]) observed usually in some strong magnetic frustrated antiferromagnets [58,59], and the characteristic of Kitaev-type frustration was reflected coincidentally. To track these changes across the whole temperature range, the ZF- μ SR spectra could be modeled by:

$$\mathbf{A}_{ZF}(t) = A_1 \cdot \left[\alpha \cos(\gamma_\mu B_{\text{int}} t + \varphi) \cdot e^{-\lambda_T t} + (1-\alpha) \cdot e^{-\lambda_L t} \right] + A_2 e^{-\lambda_{\text{tail}} t} \cdot G_{KT} \quad (2)$$

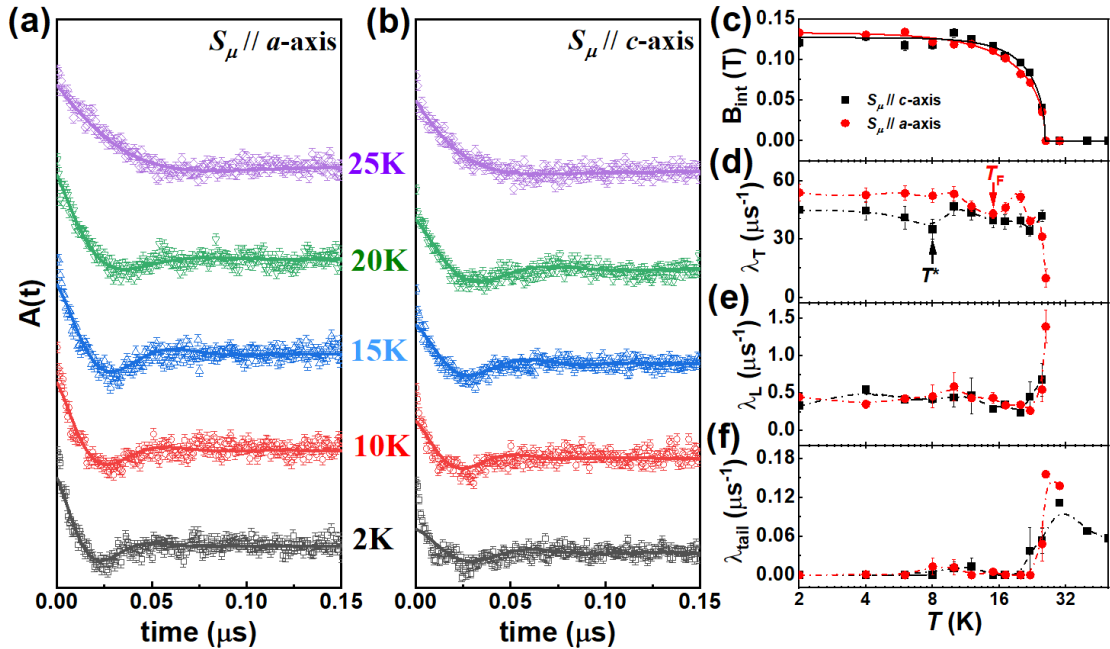


Figure 4. Zero-field μ SR study of $\text{Na}_2\text{Co}_2\text{TeO}_6$. (a) and (b) Zero-field (ZF) μ SR time spectra measured at selected temperatures (vertically displaced for clarity) with the muon-spin direction $S_\mu \parallel \mathbf{a}$ -axis in the ab plane and \mathbf{c} -axis, respectively. The solid curves represent the results of least-squares fitting using Eq. (1.3). (c)-(f) Temperature dependence of B_{int} , λ_T , λ_L , and λ_{tail} , respectively, as derived from ZF- μ SR analysis. Solid lines are fits by a phenomenological equation described in the text; dash-dotted lines are guides to the eyes. The ZF- μ SR data were collected using the M20D spectrometer.

Here, α and $1 - \alpha$ are the oscillating (i.e., transverse) and nonoscillating (i.e.,

longitudinal) fractions of the μ SR signal, λ_T and λ_L represent the transverse and longitudinal muon-spin relaxation rates, A_1 and A_2 represent the asymmetries of the two nonequivalent muon-stopping sites. The muons stopping at the second site do not undergo any precession but show only a weak relaxation, which can be described by an exponential relaxation λ_{tail} . Above T_N , the ZF- μ SR spectra show only a weak relaxation. The G_{KT} is the static Kubo-Toyabe relaxation function, normally used to describe the muon-spin relaxation due to the nuclear moments. In the magnetically ordered state, the muon-spin relaxation due to the electronic moments is significantly larger than the contribution from the nuclear moments. Therefore, below T_N the G_{KT} can be ignored in general. In our analysis, we set G_{KT} to be 1 at temperatures below T_N , Fig. S5 [42].

Usually, the changes in the magnitude of the magnetic moment can be detected by the temperature-dependent internal magnetic field $B_{\text{int}}(T)$ curves. However, the modulation of magnetic domains is related to the distribution of internal magnetic fields. The fitting parameters of ZF- μ SR spectra are summarized in Figure 4(c)-(f), which helps to distinguish the origin of these complex magnetic orders. It is worth mentioned that as the temperature changes, α is not a constant to ensure a more reasonable parameter set below T_N due to the complex competitive mechanism from two different exchange frustrations: J_1 - J_3 -type and Kitaev-type frustrations [13,33-35,41], which might trigger significant spin fluctuations accompanied by changes of spin directions, Fig. S6(c) [42]. Actually, the curves of the temperature-dependent parameter α give weak anomalies near T_F and T^* , which may mirror the modulation of magnetic domains and change the spin directions.

The $B_{\text{int}}(T)$ curves with $\mathbf{S}_\mu \parallel \mathbf{a}$ -axis and \mathbf{c} -axis present the similar features, Figure 4(c), reflecting the local ordered magnetic moment of the Co^{2+} ion and giving one distinct phase transition temperature T_N , which is compared to the temperature evolution of magnetic moment obtained by the powder neutron diffraction [39] and single-crystal neutron diffractions, Figure 1. A phenomenological equation $B_{\text{int}}(T) = B_{\text{int}}(0K) \cdot \left[1 - (T/T_N)^\gamma\right]^\delta$ could describe the $B_{\text{int}}(T)$ curves, Figure 4(c). Here, $B_{\text{int}}(0K)$ is the internal magnetic field at 0 K, γ and δ are two empirical parameters. The fitted

parameters are summarized in Table SI of the supplementary materials [42].

Interestingly, the other two anomalies at T_F and T^* can be well demonstrated by the temperature-dependent $\lambda_T(T)$ curves with both $\mathbf{S}_\mu // \mathbf{a}$ -axis and \mathbf{c} -axis which reflect the width of static magnetic field distribution at the muon-stopping site, Figure 4(d). These results suggest that the anomalies observed at T_F and T^* should be attributed to the redistribution of magnetic domains originated from three different k -vectors of the zigzag AFM order. Hence, the multi-domain structure is again supported by the ZF- μ SR results, consistent with the single-crystal neutron diffraction results, Figure 3(c).

Meanwhile, spin fluctuations can also be expressed by the longitudinal relaxation rate λ_L . As shown in the Figure 4(e), both $\lambda_L(T)$ diverge near T_N but show significant drops at $T < T_N$, indicating that spin fluctuations are the strongest close to the onset of the AFM order. At low temperatures, the λ_L becomes approximately constant that is close to $0.45 \mu\text{s}^{-1}$ in NCTO. For the promising QSL candidate YbMgGaO_4 , similar T -independent behavior with a value of $0.3 \mu\text{s}^{-1}$ at low temperatures was suggested with very strong quantum fluctuations [60]. Hence, the temperature independence of λ_L indicates the strong quantum fluctuations in NCTO. Moreover, a temperature-dependent $\lambda_{\text{tail}}(T)$ is nearly close to zero below T_N , Figure 4(f), and corresponds to a simple exponential correction originating from the low background.

We now discuss the zigzag AFM ordered ground state with the multi-domain structure, accompanied by strong quantum fluctuations in NCTO. Using the same parameters, the power-law function gives the similar $I(T)$ curves at the M and M_1 points, Figure 1(c), which presents a magnetic phase transition at T_N from PM to AFM order. The small bump at T_F , corresponding to the opening of spin-wave-excitation gap [31], only can be observed by the $I(T)$ curves of the M_1 -point, which means that the magnetic anisotropic-exchange interactions induce the non-equivalent magnetic domains at the M and M_1 points. The field-dependent intensities of magnetic reflections further confirm that the magnetic domains along the magnetic field direction are growing while other directions are suppressed. Meanwhile, the $\lambda_T(T)$ curves suggesting the modulation of magnetic domains, verify again that the domain reorientation occurs at T_F and T^* .

These results indicate that the most relevant anisotropic interactions K and Γ terms [13,33-35,41] are responsible for the highly anisotropic response to a variety of complex phases, leading to motion of magnetic domains and supporting the multi-domain structure in NCTO.

Indeed, many previous studies indicate that the Kitaev coupling K is the dominant microscopic interaction with bond-dependent anisotropic frustration and the off-diagonal exchange Γ term, another source of frustration that is also essential for understanding the Kitaev physics [13,19,28,33-35,41]. These anisotropic exchange frustrations along with the J_1 - J_3 -type frustration may lead to strong quantum fluctuations. As revealed by our μ SR measurements, NCTO reveals the superimposed muon-spin oscillations within 50 ns (Figure 4 (a) and (b)) and the λ_L becomes approximately constant, that is close to $0.45 \mu\text{s}^{-1}$ (Figure 4 (e)) at low temperatures. Taken together, our μ SR data indicate that the strong spin dynamics should be quantum at low temperatures and the opening of spin-wave-excitation gap below T_F further eliminates the contribution of thermal fluctuations. Meanwhile, these quantum fluctuations can be enhanced by applying magnetic field, which is confirmed by these observations on the broadening of the K-point where the FWHM is gradually increasing with the increasing fields, the inset of Figure 2(c). These results further support the appearance of the field-induced Kitaev QSL between 7.5 T and 10 T in NCTO [13,19,26,37], indicating that the applied magnetic fields could quickly suppress magnetically ordered states and the K term's contribution to quantum fluctuations is reflected by the magnetic fields.

In summary, we have investigated both the magnetic structure characteristics and related dynamics of ground state in NCTO. The most significant observations from our studies are that NCTO hosts a multi-domain zigzag AFM order with strong quantum fluctuations. Our findings can well reflect the exposition of microscopic origin from HK model where the coexistence of static magnetic order from the non-Kitaev interactions and dynamic quantum fluctuations from the frustrated K term indicates the highly frustrated magnetic structure.

Note added. During writing the manuscript, we noticed that the μ SR experiments, with lower resolution in the part of early time of 50 ns, have been also presented independently [61].

ACKNOWLEDGMENTS

G.T.L, T.S. and J.M. thank the financial support from the National Key Research and Development Program of China (No. 2022YFA1402702), the National Science Foundation of China (Nos. U2032213, 12004243, 12374105). J.M. thanks the interdisciplinary program Wuhan National High Magnetic Field Center (No. WHMFC 202122), Huazhong University of Science and Technology. T. S. acknowledges support from the Natural Science Foundation of Shanghai (Grant Nos. 21ZR1420500 and 21JC1402300), Natural Science Foundation of Chongqing (Grant No. CSTB-2022NSCQ-MSX1678). The work performed in the University of Tennessee (crystal growth) was supported by NSF-DMR-2003117. We acknowledge the neutron beam time from SINQ with Proposal 20222504, SNS with Proposal No. IPTS-27393.1, and ANSTO with Proposal No. P15604. We thank ACNS for the beam time, thank sample environment group at ACNS for the support. This research used resources at the Spallation Neutron Source, a DOE Office of Science User Facility operated by the Oak Ridge National Laboratory. The part of this work is based on experiments performed at the Swiss spallation neutron source SINQ, Paul Scherrer Institut, Villigen, Switzerland.

REFERENCES

- [1] A. Kitaev, *Annals of Physics* **321**, 2 (2006).
- [2] G. Jackeli and G. Khaliullin, *Phys. Rev. Lett.* **102**, 017205 (2009).
- [3] J. Chaloupka, G. Jackeli, and G. Khaliullin, *Phys. Rev. Lett.* **105**, 027204 (2010).
- [4] C. Xu, J. Feng, M. Kawamura, Y. Yamaji, Y. Nahas, S. Prokhorenko, Y. Qi, H. Xiang, and L. Bellaiche, *Phys. Rev. Lett.* **124**, 087205 (2020).
- [5] O. Tanaka, Y. Mizukami, R. Harasawa, K. Hashimoto, K. Hwang, N. Kurita, H. Tanaka, S. Fujimoto, Y. Matsuda, E. G. Moon, and T. Shibauchi, *Nature Physics* **18**, 2759 (2022).
- [6] H. Takagi, T. Takayama, G. Jackeli, G. Khaliullin, and S. E. Nagler, *Nature Reviews Physics* **1**, 264 (2019).
- [7] P. A. Maksimov and A. L. Chernyshev, *Phys. Rev. Res.* **2**, 033011 (2020).
- [8] T. Yokoi, S. Ma, Y. Kasahara, S. Kasahara, T. Shibauchi, N. Kurita, H. Tanaka, J. Nasu, Y. Motome, C. Hickey, S. Trebst, and Y. Matsuda, *Science* **373**, 568 (2021).
- [9] Y. Kasahara, T. Ohnishi, Y. Mizukami, O. Tanaka, S. Ma, K. Sugii, N. Kurita, H. Tanaka, J. Nasu, Y. Motome, T. Shibauchi, and Y. Matsuda, *Nature* **559**, 227 (2018).
- [10] A. Banerjee, J. Yan, J. Knolle, C. A. Bridges, M. B. Stone, M. D. Lumsden, D. G. Mandrus, D. A. Tennant, R. Moessner, and S. E. Nagler, *Science* **356**, 1055 (2017).
- [11] S. Hwan Chun, J.-W. Kim, J. Kim, H. Zheng, Constantinos C. Stoumpos, C. D. Malliakas, J. F. Mitchell, K. Mehlawat, Y. Singh, Y. Choi, T. Gog, A. Al-Zein, M. Moretti Sala, M. Krisch, J. Chaloupka, G. Jackeli, G. Khaliullin, and B. J. Kim, *Nature Physics* **11**, 462 (2015).
- [12] W. Yao, K. Iida, K. Kamazawa, and Y. Li, *Phys. Rev. Lett.* **129**, 147202 (2022).
- [13] Gaoting Lin, Jaehong Jeong, Chaebin Kim, Yao Wang, Qing Huang, Takatsugu Masuda, Shinichiro Asai, Shinichi Itoh, Gerrit Günther, Margarita Russina, Zhilun Lu, Jieming Sheng, Le Wang, Jiucai Wang, Guohua Wang, Qingyong Ren, Chuanying Xi, Wei Tong, Langsheng Ling, Zhengxin Liu, Liusuo Wu, Jiawei Mei, Zhe Qu, Haidong Zhou, Xiaoqun Wang, Je-Geun Park, Yuan Wan, and Jie Ma, *Nat. Commun.* **12**, 5559 (2021).
- [14] C. Broholm, R. J. Cava, S. A. Kivelson, D. G. Nocera, M. R. Norman, and T. Senthil, *Science* **367**, eaay0668 (2020).
- [15] H. Liu, J. Chaloupka, and G. Khaliullin, *Phys. Rev. Lett.* **125**, 047201 (2020).
- [16] R. Sano, Y. Kato, and Y. Motome, *Phys. Rev. B* **97**, 014408 (2018).
- [17] H. Liu and G. Khaliullin, *Phys. Rev. B* **97**, 014407 (2018).
- [18] K. Kitagawa, T. Takayama, Y. Matsumoto, A. Kato, R. Takano, Y. Kishimoto, S. Bette, R. Dinnebier, G. Jackeli, and H. Takagi, *Nature* **554**, 341 (2018).
- [19] Gaoting Lin, Qirong Zhao, Gang Li, Mingfang Shu, Yinina Ma, Jinlong Jiao, Guijing Duan, Qing Huang, Jieming Sheng, Alexander I. Kolesnikov, Lu Li, Liusuo Wu, Rong Yu, Xiaoqun Wang, Zhengxin Liu, Haidong Zhou, and Jie Ma, PREPRINT (Version 1) available at Research Square (2022).
- [20] S.-H. Do, S.-Y. Park, J. Yoshitake, J. Nasu, Y. Motome, Yong S. Kwon, D. T. Adroja, D. J. Voneshen, K. Kim, T. H. Jang, J.-H. Park, Kwang-Yong Choi, and Sungdae Ji, *Nature Physics* **13**, 1079 (2017).
- [21] S. K. Choi, R. Coldea, A. N. Kolmogorov, T. Lancaster, Mazin, II, S. J. Blundell,

P. G. Radaelli, Y. Singh, P. Gegenwart, K. R. Choi, S.-W. Cheong, P. J. Baker, C. Stock, and J. Taylor, *Phys. Rev. Lett.* **108**, 127204 (2012).

[22] T. Halloran, F. Desrochers, E. Z. Zhang, T. Chen, L. E. Chern, Z. Xu, B. Winn, M. Graves-Brook, M. B. Stone, A. I. Kolesnikov, Yiming Qiu, Ruidan Zhong, Robert Cava, Yong Baek Kim, and Collin Broholm, *Proceedings of the National Academy of Sciences* **120**, e2215509119 (2023).

[23] X. Zhang, Y. Xu, T. Halloran, R. Zhong, C. Broholm, R. J. Cava, N. Drichko, and N. P. Armitage, *Nature Materials* **22**, 58 (2022).

[24] S. M. Winter, *Journal of Physics: Materials* **5**, 045003 (2022).

[25] X. Li, Y. Gu, Y. Chen, V. O. Garlea, K. Iida, K. Kamazawa, Y. Li, G. Deng, Q. Xiao, X. Zheng, Z. Ye, Y. Peng, I. A. Zaliznyak, J. M. Tranquada, and Y. Li, *Phys. Rev. X* **12**, 041024 (2022).

[26] S. Zhang, S. Lee, A. J. Woods, W. K. Peria, S. M. Thomas, R. Movshovich, E. Brosha, Q. Huang, H. Zhou, V. S. Zapf, and M. Lee, *Phys. Rev. B* **108**, 064421 (2023).

[27] W. Yao, Y. Zhao, Y. Qiu, C. Balz, J. R. Stewart, J. W. Lynn, and Y. Li, *Phys. Rev. Res.* **5**, L022045 (2023).

[28] W. G. F. Krüger, W. Chen, X. Jin, Y. Li, and L. Janssen, *Phys. Rev. Lett.* **131**, 146702 (2023).

[29] G. Xiao, Z. Xia, Y. Song, and L. Xiao, *J. Phys. Condens. Matter.* **34**, 075801 (2022).

[30] C. H. Lee, S. Lee, Y. S. Choi, Z. H. Jang, R. Kalaivanan, R. Sankar, and K. Y. Choi, *Phys. Rev. B* **103**, 214447 (2021).

[31] W. Chen, X. Li, Z. Hu, Z. Hu, L. Yue, R. Sutarto, F. He, K. Iida, K. Kamazawa, W. Yu, X. Lin, and Y. Li, *Phys. Rev. B* **103**, L180404 (2021).

[32] W. Yao and Y. Li, *Phys. Rev. B* **101**, 085120 (2020).

[33] C. Kim, J. Jeong, G. Lin, P. Park, T. Masuda, S. Asai, S. Itoh, H. S. Kim, H. Zhou, J. Ma, and Je-Geun Park, *J. Phys. Condens. Matter.* **34**, 045802 (2022).

[34] A. M. Samarakoon, Q. Chen, H. Zhou, and V. O. Garlea, *Phys. Rev. B* **104**, 184415 (2021).

[35] M. Songvilay, J. Robert, S. Petit, J. A. Rodriguez-Rivera, W. D. Ratcliff, F. Damay, V. Balédent, M. Jiménez-Ruiz, P. Lejay, E. Pachoud, A. Hadj-Azzem, V. Simonet, and C. Stock, *Phys. Rev. B* **102**, 224429 (2020).

[36] X. Hong, M. Gillig, R. Henrich, W. Yao, V. Kocsis, A. R. Witte, T. Schreiner, D. Baumann, N. Pérez, A. U. B. Wolter, Y. Li, B. Büchner, and C. Hess, *Phys. Rev. B* **104**, 144426 (2021).

[37] Patrick Pilch, Laur Peedu, Anup Kumar Bera, S. M. Yusuf, Urmas Nagel, Toomas Ro~om, and Z. Wang, *arXiv:2308.00631v1* (2023).

[38] N. Li, R. R. Neumann, S. K. Guang, Q. Huang, J. Liu, K. Xia, X. Y. Yue, Y. Sun, Y. Y. Wang, Q. J. Li, Y. Jiang, J. Fang, Z. Jiang, X. Zhao, A. Mook, J. Henk, I. Mertig, H. D. Zhou, and X. F. Sun, *Phys. Rev. B* **108**, 140402 (2023).

[39] A. K. Bera, S. M. Yusuf, A. Kumar, and C. Ritter, *Phys. Rev. B* **95**, 094424 (2017).

[40] E. Lefrançois, M. Songvilay, J. Robert, G. Nataf, E. Jordan, L. Chaix, C. V. Colin, P. Lejay, A. Hadj-Azzem, R. Ballou, and V. Simonet, *Phys. Rev. B* **94**, 214416 (2016).

[41] A. L. Sanders, R. A. Mole, J. Liu, A. J. Brown, D. Yu, C. D. Ling, and S. Rachel, *Phys. Rev. B* **106**, 014413 (2022).

[42] See Supplemental Material at [http://link.aps.org/supplemental/...](http://link.aps.org/supplemental/) for additional methods, data, and analyses.

[43] M. B. Stone, J. L. Niedziela, D. L. Abernathy, L. DeBeer-Schmitt, G. Ehlers, O. Garlea, G. E. Granroth, M. Graves-Brook, A. I. Kolesnikov, A. Podlesnyak, B. Winn, *Rev. Sci. Instrum.* **85**, 045113 (2014).

[44] G. E. Granroth, A. I. Kolesnikov, T. E. Sherline, J. P. Clancy, K. A. Ross, J. P. C. Ruff, B. D. Gaulin, and S. E. Nagler, *Journal of Physics: Conference Series* **251**, 012058 (2010).

[45] C. M. Wu, G. Deng, J. S. Gardner, P. Vorderwisch, W. H. Li, S. Yano, J. C. Peng, and E. Imamovic, *Journal of Instrumentation* **11**, P10009 (2016).

[46] A. Suter and B. M. Wojek, *Musrfit: A free platform-independent framework for μ SR data analysis*, *Phys. Procedia* **30**, 69 (2012).

[47] V. O. Garlea, R. Jin, D. Mandrus, B. Roessli, Q. Huang, M. Miller, A. J. Schultz, and S. E. Nagler, *Phys. Rev. Lett.* **100**, 066404 (2008).

[48] M. F. Collins, *Magnetic Critical Scattering* (Oxford university press, New York, (1989).

[49] J. Rodríguez-Carvajal and J. Villain, *Comptes Rendus Physique* **20**, 770 (2019).

[50] H. Saito, F. Kon, H. Hidaka, H. Amitsuka, C. Kwanghee, M. Hagihala, T. Kamiyama, S. Itoh, and T. Nakajima, *Phys. Rev. B* **108**, 094440 (2023).

[51] N. D. Khanh, T. Nakajima, S. Hayami, S. Gao, Y. Yamasaki, H. Sagayama, H. Nakao, R. Takagi, Y. Motome, Y. Tokura, T. Arima, and S. Seki, *Advanced Science* **9**, 2105452 (2022).

[52] R. Takagi, J. S. White, S. Hayami, R. Arita, D. Honecker, H. M. Rønnow, Y. Tokura, and S. Seki, *Science Advances* **4**, eaau3402 (2018).

[53] W. C. Pyeongjae Park, Chaebin Kim, Yeochan An, Yoon-Gu Kang, Maxim Avdeev, Romain Sibille, Kazuki Iida, Ryoichi Kajimoto, Ki Hoon Lee, Woori Ju, En-Jin Cho, Han-Jin Noh, Myung Joon Han, Shang-Shun Zhang, Cristian D. Batista, and Je-Geun Park, *arXiv:2303.03760* (2023).

[54] J. Ma, Y. Kamiya, T. Hong, H. B. Cao, G. Ehlers, W. Tian, C. D. Batista, Z. L. Dun, H. D. Zhou, and M. Matsuda, *Phys. Rev. Lett.* **116**, 087201 (2016).

[55] Y. Shen, Y. D. Li, H. Wo, Y. Li, S. Shen, B. Pan, Q. Wang, H. C. Walker, P. Steffens, M. Boehm, Y. Hao, D. L. Quintero-Castro, L. W. Harriger, M. D. Frontzek, L. Hao, S. Meng, Q. Zhang, G. Chen, and J. Zhao, *Nature* **540**, 559 (2016).

[56] Y. Shen, Y. D. Li, H. C. Walker, P. Steffens, M. Boehm, X. Zhang, S. Shen, H. Wo, G. Chen, and J. Zhao, *Nat. Commn.* **9**, 4138 (2018).

[57] X. Y. Zhu, H. Zhang, D. J. Gawryluk, Z. X. Zhen, B. C. Yu, S. L. Ju, W. Xie, D. M. Jiang, W. J. Cheng, Y. Xu, M. Shi, E. Pomjakushina, Q. F. Zhan, T. Shiroka, and T. Shang, *Phys. Rev. B* **105**, 014423 (2022).

[58] M. T. Rovers, P. P. Kyriakou, H. A. Dabkowska, G. M. Luke, M. I. Larkin, and A. T. Savici, *Phys. Rev. B* **66**, 174434 (2002).

[59] E. M. Kenney, M. M. Bordelon, C. Wang, H. Luetkens, S. D. Wilson, and M. J. Graf, *Phys. Rev. B* **106**, 144401 (2022).

[60] Yuesheng Li, Devashibhai Adroja, Pabitra K. Biswas, Peter J. Baker, Qian Zhang, Juanjuan Liu, Alexander A. Tsirlin, Philipp Gegenwart, and Qingming Zhang, *Phys.*

Rev. Lett. **117**, 097201 (2016).

[61]Ping Miao, Xianghong Jin, Weiliang Yao, Yue Chen, Akihiro Koda, Zhenhong Tan, Wu Xie, Wenhui Ji, Takashi Kamiyama, and Y. Li, arXiv:2307.16451v1 (2023).

Supplementary Material for “Static magnetic order with strong quantum fluctuations in spin-1/2 honeycomb magnet $\text{Na}_2\text{Co}_2\text{TeO}_6$ ”

Inelastic neutron scattering. For the experiments on SEQUOIA time-of-flight spectrometer at the Spallation Neutron Source, Oak Ridge National Laboratory, USA, measurements at 2 K with applied field $B = 0$ T and 4 T were performed by rotating the sample around vertical axis (sample a^* -axis) in steps of 1° with $E_i = 18$ meV and choppers in high-resolution mode, yielding a full-width at half-maximum (FWHM) elastic energy resolution of about 0.41 meV. In order to subtract the background, the INS data were collected at 90 K. The constant-Q scans of the K-point $(1/3, 1/3, 0)$ at 1.5 K with applied field B up to 4 T and $B \parallel [-1,1,0]$ direction were measured on Cold Triple Axis Spectrometer SIKA at the ANSTO, Australia. For the measurements on SIKA, data were collected using a fixed final-energy mode with $E_f = 5.0$ meV.

Muon spin rotation or relaxation. For the experiments on M20D surface muon beam line at TRIUMF, the aligned NCTO crystals were positioned on a thin silver tape, Figure S2(a) and (b), with their c axes parallel to the muon momentum direction. We aimed at studying the temperature evolution of the magnetically ordered phase and the dynamics of spin fluctuations. For the experiments on GPS instrument, since NCTO is quite thin and flat, we simply used two layers of samples and then wrapped them with Kapton foil, Figure S2(c) and (d). The muon momentum is always parallel to the c -axis of the crystal. The muon spin should be tuned in the ab -plane (TRAN mode) or along c -axis (LONG mode). Based on the wTF- μ SR data, we could determine the temperature evolution of the magnetic volume fraction. For the wTF- μ SR measurements, the applied magnetic field was perpendicular to the muon-spin direction.

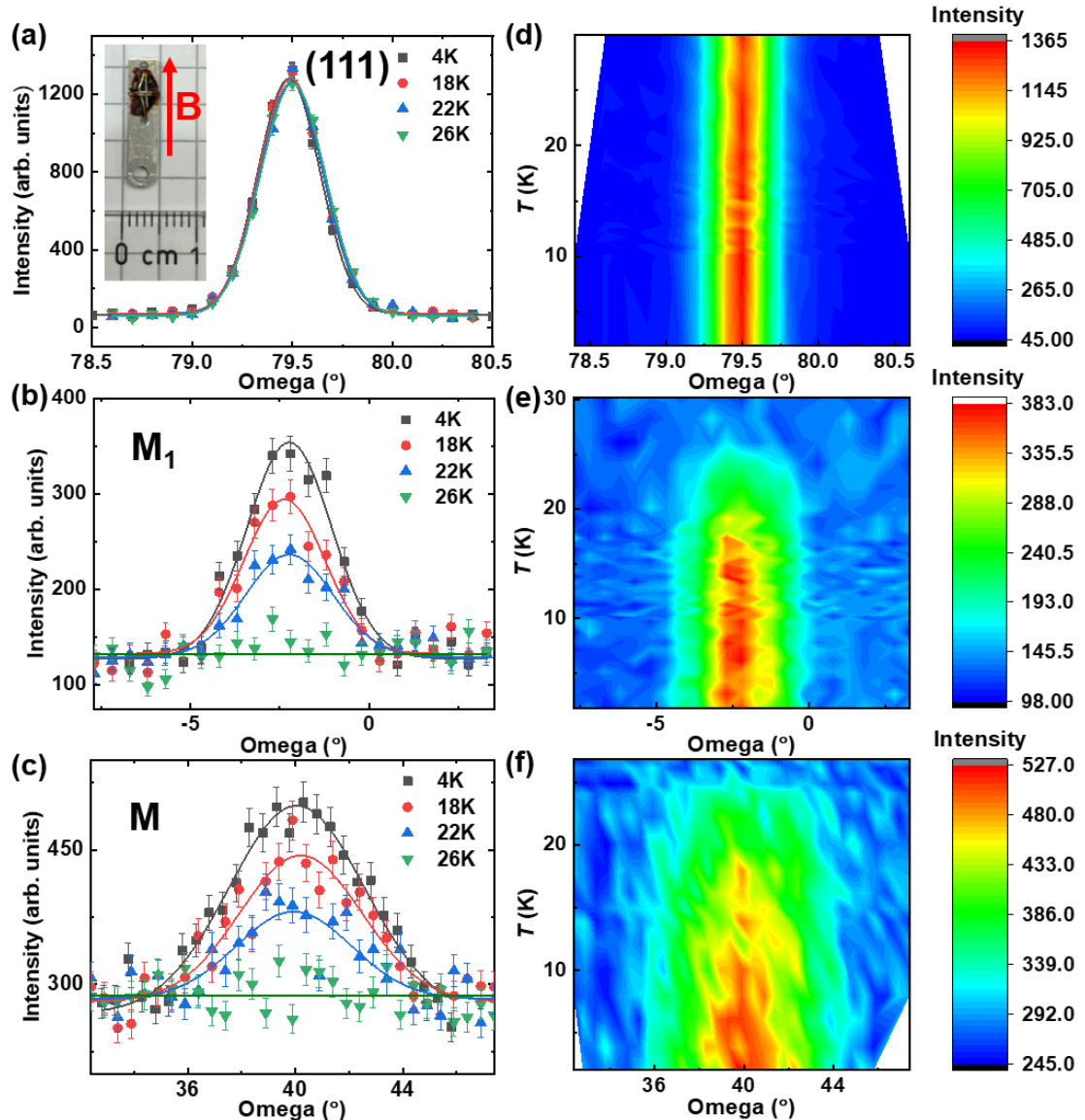


Figure S1. Single-crystal neutron diffraction of NCTO at the ZEBRA diffractometer. (a), (b), and (c) Zero-field temperature dependence of the nuclear peak (111), magnetic peak M₁ (-0.5, 0.5, 1) and M (0.5, 0, 1) at selected temperatures. The data collected at each temperature were fitted by a Gaussian function (the solid lines) to obtain an integrated intensity plotted in Figure 1. Inset: the sample used for the single crystal neutron diffraction experiment with the magnetic field applying along [-1, 1, 0] direction. (d), (e), and (f) The contour maps of (111), (-0.5, 0.5, 1), and (0.5, 0, 1) peaks. Apparently, there is no lattice distortion or ferromagnetic contribution with temperature evolution from (d).

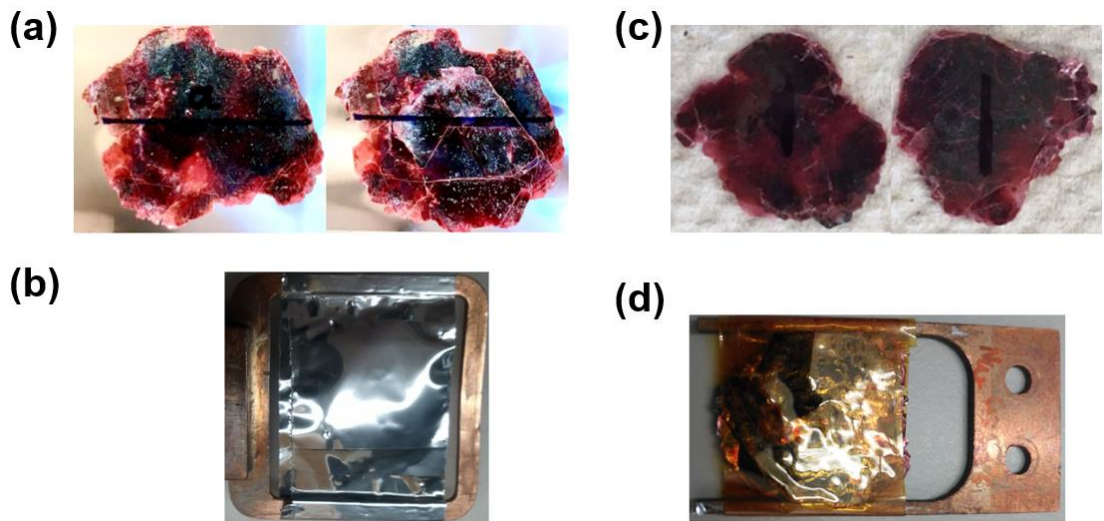


Figure S2. The photos of measured samples for μ SR. (a) The sample photos for the μ SR on M20D spectrometer. The scribed lines on the samples mark the a -axis of the crystal. (b) The aligned NCTO crystals are positioned on a thin silver tape for M20D spectrometer. (c) The sample photos for the μ SR on GPS spectrometer. (d) The aligned NCTO crystals are wrapped with Kapton foil for GPS spectrometer. The scribed lines on the samples mark the a -axis of the crystal.

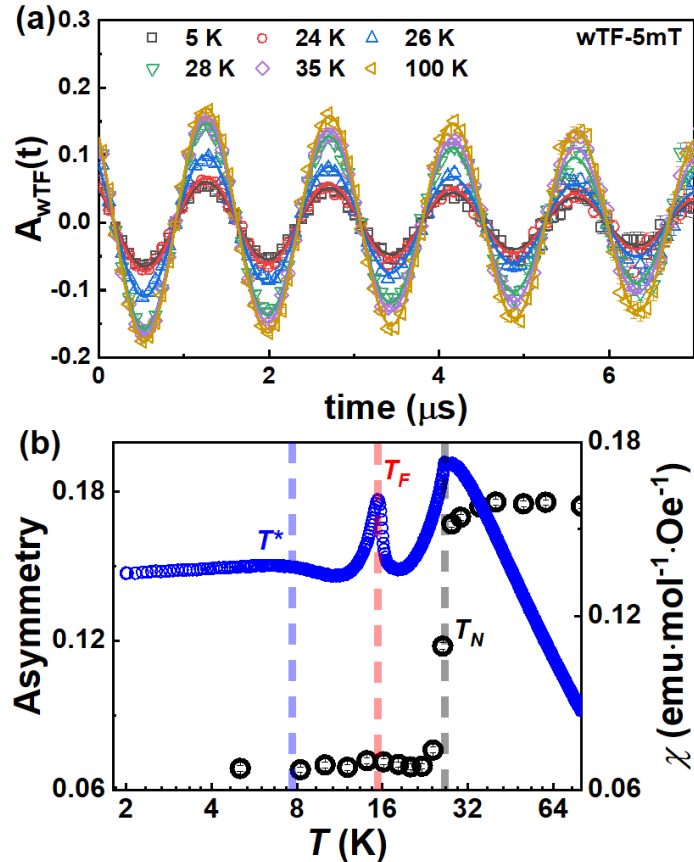


Figure S3. (a) Time-domain wTF- μ SR spectra were collected at different temperatures with a weak transverse field of 5 mT, which was acquired at GPS spectrometer. The solid lines are the fitted results by the Eq. (1); (b) Temperature-dependent A_{NM} asymmetry (left axis, black and red curves) was obtained from the fit of wTF- μ SR spectra. For comparison, we present the zero-field cooling (ZFC) magnetic susceptibility $\chi(T)$ curve at $B = 0.01$ T (right axis and blue curve) with $\mathbf{B} \parallel \mathbf{a}^*$ -axis; The magnetic susceptibility data were taken from Ref. [19] of main text.

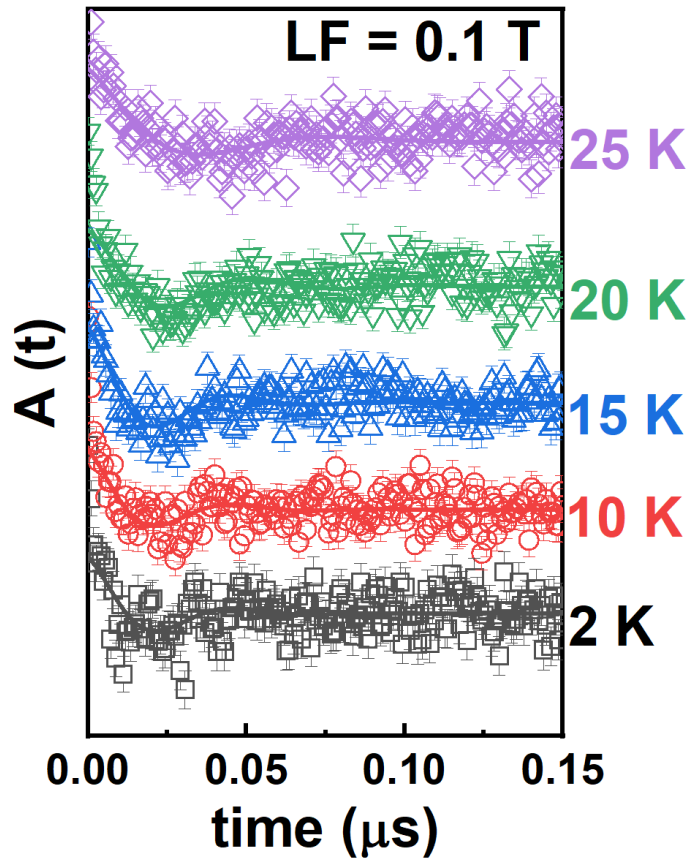


Figure S4. The μ SR time spectra with $LF = 0.1$ T measured at selected temperatures (vertically displaced for clarity) with the muon-spin direction $S_\mu \parallel c$ -axis. The solid curves represent the results of least-squares fitting using Eq. (2) of main text. Such fast depolarization and superimposed oscillations within 50 ns originated from the AFM order can be confirmed by the μ SR time spectra with $LF = 0.1$ T.

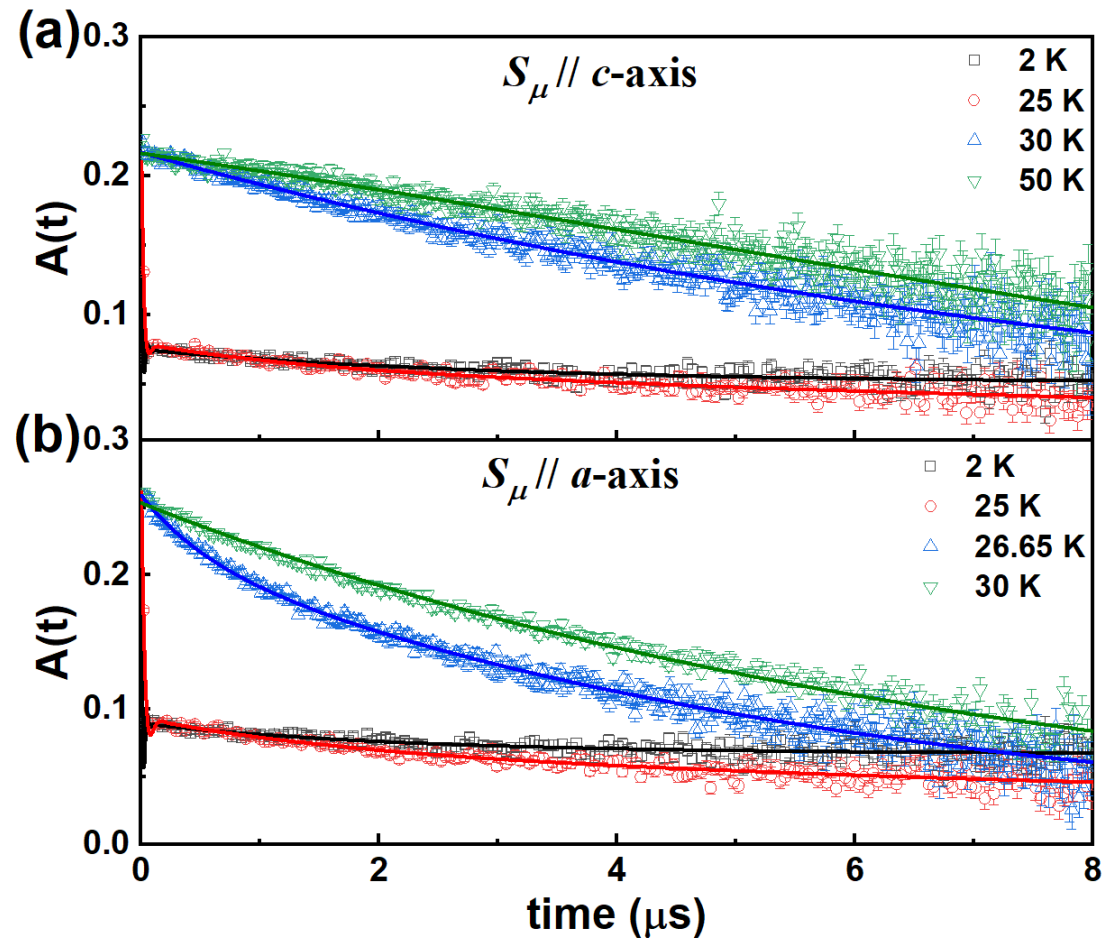


Figure S5. Zero-field μ SR data of $\text{Na}_2\text{Co}_2\text{TeO}_6$ at selected temperatures from high-temperature paramagnetic state to antiferromagnetic ground state. The data can be well described by the Eq. (2) of main text.

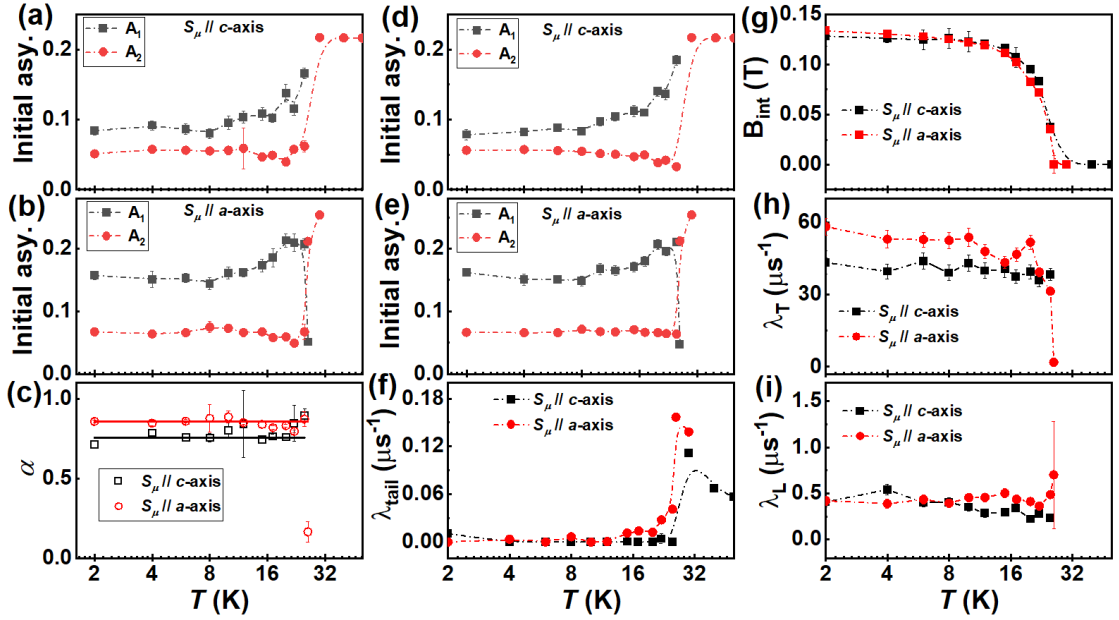


Figure S6. The fitted parameters by the Eq. (2) of main text. (a) and (b) The temperature-dependent initial asymmetry A_1 and A_2 are obtained by the unconstrained α values of the Eq. (2), which are shown in (c). (d)-(i) Temperature dependence of initial asymmetry, λ_{tail} , B_{int} , λ_T , and λ_L , respectively, as derived from ZF-μSR analysis with constant values of 0.755 for $S_\mu \parallel c\text{-axis}$ and 0.8567 for $S_\mu \parallel a\text{-axis}$. The dash-dotted lines are guides to the eyes.

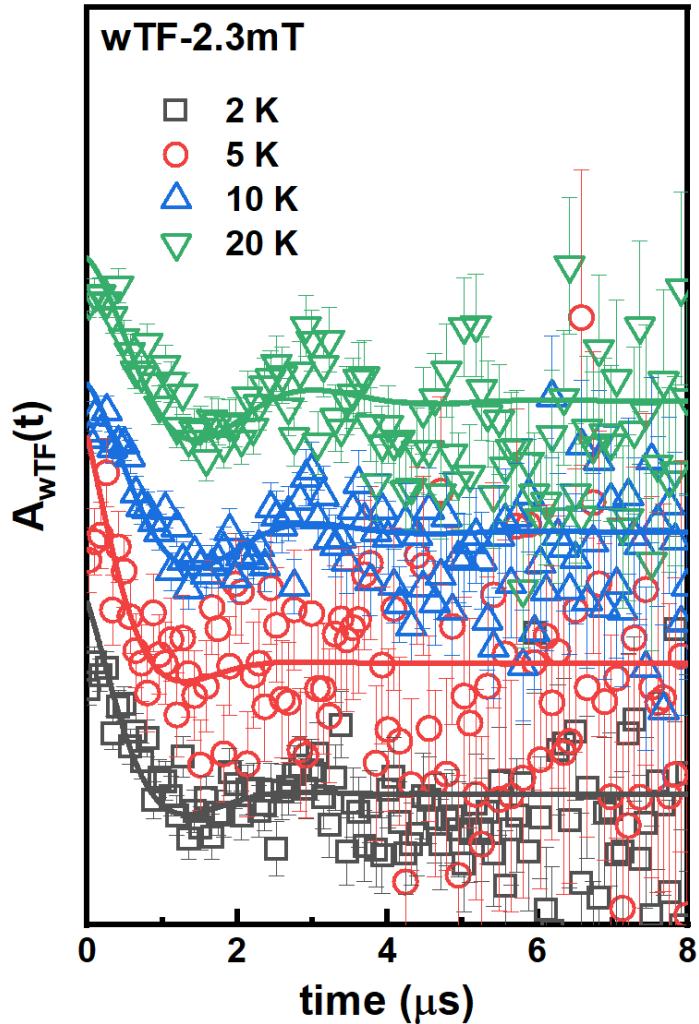


Figure S7. Time-domain wTF- μ SR spectra were collected with a weak transverse field of 2.3 mT carried out at M20D below $T_N \sim 26$ K. The solid lines are the fitted results by the Eq. (1) of main text. Due to the weak oscillation, it is difficult to maintain consistency. Hence, we fixed the phase and internal field below T_N that are from the results of 50 K, where the phase is -9.81 and the internal field is 23.621 Oe.

TABLE SI. Summary of the NCTO single-crystal parameters obtained by means of magnetization and μ SR measurements.

$\chi(T)$		ZF- μ SR $S_\mu \parallel a$ -axis	ZF- μ SR $S_\mu \parallel c$ -axis
T_N (K)	26	25.8	25.8
T_F (K)	15	15	/
T^* (K)	7	/	8
B_{int} (T)	/	0.13	0.127
γ	/	1.93	3.16
δ	/	0.47	0.47